Proceedings of the ASME 2011 International Design Engineering Technical Conferences & Computers and Information in Engineering Conference
IDETC/CIE 2011
August 28-31, 2011 Washington, DC, USA

DETC2011-48276

7-DOF CABLE-DRIVEN HUMANOID ROBOTIC ARM

Jun Ding
Mechanical Engineering, Ohio University
Athens, Ohio, USA
jd249108@ohio.edu

Robert L. Williams II
Mechanical Engineering, Ohio University
Athens, Ohio, USA
williar4@ohio.edu

ABSTRACT

The purpose of this paper is to study a 7-DOF humanoid cable-driven robotic arm, implement kinematics and dynamics analysis, present different cable-driven designs and evaluate their merits and drawbacks. Since this is a redundant mechanism, kinematics optimization is used to avoid joint limits, singularities and obstacles. Cable kinematics analysis studies the relationships between cable length and the end-effector pose**.** This is a design modified from the literature. Several new designs are compared in pseudostatics analysis of the arm and a favorable design is suggested in terms of motion range and the cable tensions. Linear programming is used to optimize cable tensions. Dynamics analysis shows that the energy consumption of a cable-driven arm is much less than that of traditional motor-driven arm. Cable-driven robots have potential benefits but also some limitations.

INTRODUCTION

An arm model with 7 DOF is often proposed for spatial robots. However, typically the actuators of the conventional robot are directly installed on the joints. It not only increases the moving weight and inertia of robot, but also greatly reduces its load capacity. At the same time, this type of design also cannot be used for high-speed motion and rapid response of a robot. However, a cable-driven method introduces a concept to overcome the disadvantages of conventional robot in motion performance (Chen et al., 2006).

The cable-driven structure is a kind of parallel mechanism transmitting force and motion by cables. There are several advantages for it such as lower weight, higher rigidity, higher accuracy and higher load capacity, compared with conventional serial robots. It can also be used in high-speed motion of a robot. Therefore, many researchers have paid attention to this area recently.

For 7 DOF redundant robotic arms, the inverse kinematics is not a difficult problem for researchers. Williams (1992) specified a certain variable to reduce 1 DOF and make this underconstrained problem into a constrained problem, so the solutions are unique. However, this method has its own limitations and is not suitable for general cases. Also, standard linear solution techniques cannot be used in this problem because the Jacobian matrix is not square. Williams (1994) proposed the general redundant solution to solve the problem. Because there are infinite solutions for this underconstrained problem, optimization should be used to improve the behavior of the motion of manipulator, in addition to producing the required motion. Several objective functions are used to avoid joint limits, singularities and obstacles (Liegeois, 1977; Williams, 1994).

There are not many published papers about cable-driven mechanism design. To realize the force-closure of the cable-driven mechanism, redundant forces are required because cables can only be pulled unilaterally in tension. In order to generate n DOF motion in one joint, at least n+1 cables are needed as actuating elements (Yang et al., 2005). Yang et al. (2005) proposed a design to use six cables to drive a spherical joint with 3 DOF. In this design, the shoulder and wrist joints of the 7 DOF manipulator are driven by six cables each, and the elbow joint is driven by two cables. They also discussed the kinematic relationship between the cable lengths and the poses of end-effector of this humanoid robotic arm. Although this design provides the robotic arm with advantages of high dexterity and large reachable workspace, it is complicated to control the arm because of the high redundancy of its spherical joints. Chen et al. (2006) proposed another design to drive the shoulder and wrist joints by four cables each, and the elbow joint by two cables. This design reduces the redundancy of spherical joints. However, the cables that control motions of elbow and wrist joints all go through the holes in the moving

platform of shoulder joint, which affects the motion of shoulder joint and increases the complexity of controlling it.

For cable-driven robots, it is critical to always maintain positive cable tensions in the motion. Williams et al. (2006) used a MATLAB function *lsqnonneg*, which solves the least-squares problem to maintain all non-negative cable tensions. However, this function is not reliable because in some cases it will still give negative solutions for cable tensions, which is not allowed in cable-driven mechanisms. Additionally, Borgstrom et al. (2009) suggested Linear Programming (LP) as an approach to optimize cable tensions for cable-driven robots.

ARM MODEL

A 7-DOF arm model and its DH Parameters (Venkatayogi, 2007) are used in this paper. As shown in Fig. 1, the model attached with eight frames includes 3 DOF for shoulder, 1 DOF for elbow and 3 DOF for wrist. Frame 0 is a fixed frame shown in Fig. 1. Frames 1 and 0 overlap when the rotational angle θ_1 is equal to zero. Hand is considered as one link and fingers are not included in this model.

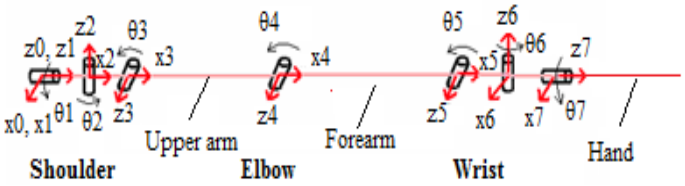

Figure 1. 7-DOF ARM MODEL (Venkatayogi, 2007)

KINEMATICS

Kinematics of the robotic arm includes forward pose kinematics, forward velocity kinematics and inverse velocity kinematics.

Forward Pose Kinematics

Forward pose kinematics is the calculation of end-effector (hand) pose of robotic arm with known rotational angles in each frame. The end-effector pose can be obtained by multiplying homogeneous transformation matrices between frames:

$$[{}^0_H T] = [{}^0_1 T][{}^1_2 T][{}^2_3 T][{}^3_4 T][{}^4_5 T][{}^5_6 T][{}^6_7 T][{}^7_H T] \quad (1)$$

Forward Velocity Kinematics

Forward velocity kinematics is the calculation of the Cartesian velocity of end-effector with known joint rates. The Cartesian velocity of end-effector can be obtained by

$$^m\{\dot{X}\} = {}^m J\{\dot{\theta}\} \quad (2)$$

where $^m J$ is the Jacobian matrix based on the Frame m; $\dot{\theta}$ is joint rates.

Inverse Velocity Kinematics

Inverse velocity kinematics is a problem of solving the linear equation for the joint rates with given Cartesian velocity of end-effector. The general redundant solution (Williams, 1994) is used for solving this problem:

$$\dot{\theta} = J^*\dot{X} + k(I_n - J^* J)\nabla H \quad (3)$$

The first term $J^*\dot{X}$ is the particular solution. The second term $k(I_n - J^* J)\nabla H$ is the homogeneous solution causing zero motion of the end-effector. The matrix J^* is the Moore-Penrose pseudoinverse of Jacobian matrix. The vector ∇H is the gradient of an objective function of joint angles. The gain k is positive to maximize H and negative to minimize H. The singularities of the arm model are obtained by $|JJ^T|=0$ (Williams, 1994). Different objective functions can be used for different optimizations.

CABLE-DRIVEN ROBOTIC ARMCONCEPT DESIGN

The typical 7 DOF cable-driven robotic arm includes two spherical joints (shoulder and wrist) with 3 DOF for each and one revolute joint (elbow) with 1 DOF. A spherical joint with four cables is proposed by Chen et al. (2006). The detailed information of the design is listed as follows: The main surface of platform $P_1P_2P_3P_4$ is a square with side length $2lc$. The thickness of platform is d. The platform and a supporting bar are connected by a ball joint. The platform can rotate about the ball joint by pulling the four cables connected to it. Those cables go through holes B_1, B_2, B_3, B_4 in a beam and connect to motors in a fixed base. Actually, B_1 and B_2 are the same hole so are B_3 and B_4. In the original design (Chen et al. 2006), it doesn't specify the lengths of $2lb$ and $2lc$.

Based on this design, many designs come up: First, there are three designs—Design 1A, 1B and 1C shown in Fig. 2 by specifying the relation between the lengths of lb and lc. Second, there are other three designs—Design 2A, 2B and 2C by rotating the beam by 90° as shown in Fig. 2. Third, there is one more design (Design 3A) by changing the surface of the beam to a square instead of a rectangle as shown in Fig. 2. However, Design 3A has more limitations in motion range than others so it will not be considered in the following analysis. For the elbow joint, the design with two cables proposed by Yang et al. (2005) is used here. Statics analysis and motion ranges will be discussed in the following sections.

STATICS ANALYSIS

An approach that calculates the coordinates of points in the moving platform of a spherical joint with known rotational angles of three frames (Chen et al., 2006**)** is used in the process of statics analysis. In order to make the problem easier to solve, statics of the whole arm will be analyzed part by part separately.

First, the hand is analyzed; its free body diagram is shown in Fig. 3. The weight of the moving platform $Q_7Q_8Q_9Q_{10}$ is G_4 and its side length is $2lq$. The length of R_7R_9 in the beam is $2lp$. The length of the supporting bar is lg. A ball joint is used to connect the supporting bar with the platform $Q_7Q_8Q_9Q_{10}$. The weight of the hand is G_5. The force exerted by the supporting bar on the platform is $\vec{f_6}$. The scalars t_7, t_8, t_9, t_{10} are the magnitude of cable tensions for the four cables. To maintain

static equilibrium of forces exerted on the hand, the equation can be expressed by

$$\sum_{i=7}^{10}(L_i/l_i \cdot t_i) + \vec{f_6} + \vec{G_5} + \vec{G_4} = 0_{3\times1} \quad (4)$$

where L_i/l_i is a unit vector along the direction of the cable tension and $L_i/l_i \cdot t_i$ is the vector of cable tension. To maintain static equilibrium of torques about point I (the ball joint), the equation is

$$\sum_{i=7}^{10}(\vec{IQ_i} \times (L_i/l_i \cdot t_i)) + \vec{IJ} \times \vec{G_5} = 0_{3\times1} \quad (5)$$

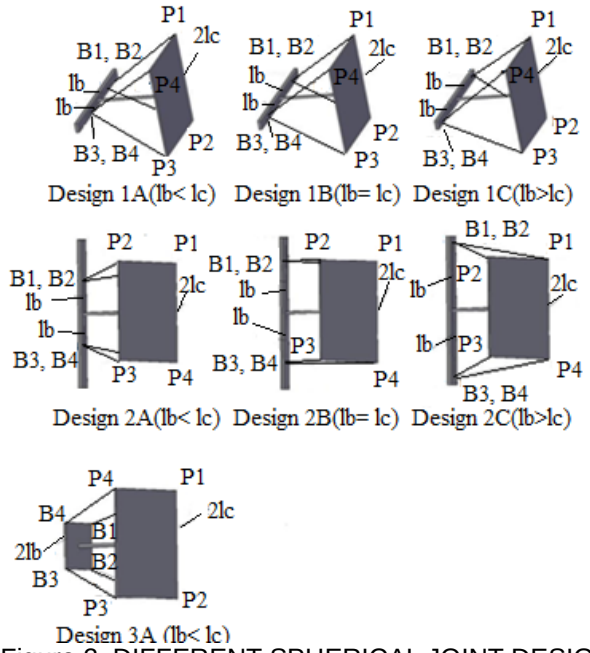

Figure 2. DIFFERENT SPHERICAL JOINT DESIGNS

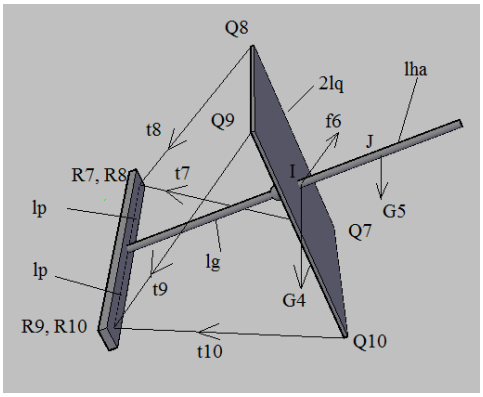

Figure 3. FREE BODY DIAGRAM OF HAND

All vectors in Eqn. (4) and Eqn. (5) are expressed in Frame 0 (a fixed frame). There are seven unknowns in those equations including t_7, t_8, t_9, t_{10} and the x, y, z components of $\vec{f_6}$. And there are three equations in each of those equations so there are six equations in total. This is an underconstrained problem because there are more unknowns than equations. Therefore, it is possible to minimize the sum of the cable tensions of four cables by linear programming function *linprog* in MATLAB. In this case the objective function is min $f^T t = t_7 + t_8 + t_9 + t_{10}$ and the lower bound of cable tension should be bigger than zero because cables can only provide positive tensions. The upper bound is obtained by the limit of cable tension divided by a safety factor. The optimal solution of cable tensions and the solution of the three components of $\vec{f_6}$ are obtained by this method.

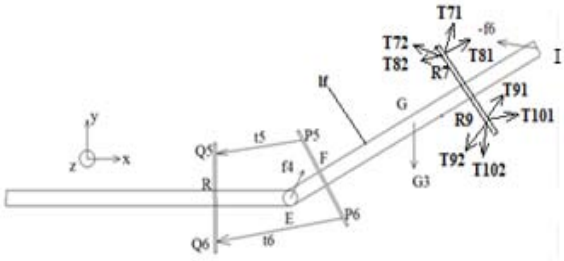

Figure 4. FREE BODY DIAGRAM OF FOREARM

Second, consider the forearm. Its free body diagram is shown in Fig. 4. In the figure, $-\vec{f_6}$ is reaction force of $\vec{f_6}$ in Fig. 3. The cables 7, 8, 9 and 10 in Fig. 3 that control the motion of the hand go through the holes R_7 and R_9 in the beam fixed in the forearm and connect directly with four motors in a fixed base. $\vec{T}_{j1}$ and $\vec{T}_{j2}$ are forces applied on the beam by the tensions of the four cables (j=7, 8, 9, 10). Those cable tensions are obtained from statics analysis of the hand. Frictions between cables and holes are not considered in this paper. The weight of the beam is negligible. Point G is the center of gravity of the forearm and G_3 is the weight of the forearm. The beam P_5P_6 is perpendicular and fixed to forearm EI. The beam is driven by two cables P_5Q_5 and P_6Q_6 and it rotates around a revolute joint E with the forearm. The two cables go through the holes Q_5, Q_6 and connect directly to the motors in the fixed base. The scalars t_5 and t_6 are magnitudes of these cable tensions. The force $\vec{f_4}$ is exerted on the forearm by the upper arm. In order to maintain static equilibrium of forces exerted on the forearm, the equation can be expressed by

$$\sum_{i=5}^{6}(L_i/l_i \cdot t_i) + \vec{G_3} + \vec{f_4} - \vec{f_6} + \sum_{j=7}^{10}(\vec{T}_{j1} + \vec{T}_{j2}) = 0_{3\times1} \quad (6)$$

In order to maintain static equilibrium of torques about joint E, the equation can be expressed by

$$\left\{\sum_{i=5}^{6}(\vec{EP_i} \times (L_i/l_i \cdot t_i)) + \vec{EG} \times \vec{G_3} + \vec{EI} \times (-\vec{f_6}) + \vec{ER_7} \times \sum_{j=7}^{8}(\vec{T}_{j1} + \vec{T}_{j2}) + \vec{ER_9} \times \sum_{k=9}^{10}(\vec{T}_{k1} + \vec{T}_{k2})\right\}^T \cdot \begin{bmatrix}0\\0\\1\end{bmatrix} = 0_{1\times1} \quad (7)$$

Because the revolute joint E can only rotate along the z axis, it can only balance torques in the z direction. That is why Eqn. (7) only contains equation of torques in the z direction. Since $\vec{f_6}$ is known from the analysis of the hand, there are only five unknowns and four equations in Eqn. (6) and (7). The five unknowns are t_5, t_6 and three components of $\vec{f_4}$. This is still an underconstrained problem. The optimal solution for t5, t6 and

solution for $\vec{f}_4$ can be obtained from those equations by linear programming. The torques in the x and y axes will transfer to upper arm by this revolute joint. They can be calculated by

$$\tau_1 = \left\{\sum_{i=5}^{6}(\overrightarrow{EP_i} \times (L_i/l_i \cdot t_i)) + \overrightarrow{EG} \times \vec{G}_3 + \overrightarrow{EI} \times \left(-\vec{f}_6\right) + \overrightarrow{ER}_7 \times \sum_{j=7}^{8}(\vec{T}_{j1} + \vec{T}_{j2}) + \overrightarrow{ER}_9 \times \sum_{k=9}^{10}(\vec{T}_{k1} + \vec{T}_{k2})\right\}^T \cdot N \quad (8)$$

where $N=\begin{bmatrix}1 & 0 & 0\\ 0 & 1 & 0\\ 0 & 0 & 0\end{bmatrix}$ and τ_1 is a 1×3 vector. The first two items of τ_1 are the torques expressed in the x and y axes of Frame 3 of the arm model. The third item is zero because torques in the z axis can be balanced by the revolute joint.

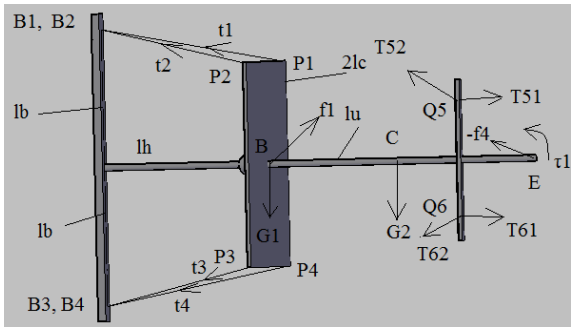

Figure 5. FREE BODY DIAGRAM OF UPPER ARM

Third, the statics of the upper arm is analyzed here. The free body diagram is shown in Fig. 5. In the figure, τ_1 is the torque transferred by the revolute joint in elbow. And $-\vec{f}_4$ is reaction force of $\vec{f}_4$ in Fig. 4. The cables 5 and 6 in Fig. 4 that control the motion of the forearm go through the holes Q_5 and Q_6 in the beam fixed in the upper arm and connect directly with two motors in a fixed base. $\vec{T}_{i1}$ and $\vec{T}_{i2}$ are forces applied on the beam by the two cable tensions (i=5, 6). The cable tensions are obtained from statics analysis of the forearm. The weight of the beam is negligible. The vector G_2 is the weight of the upper arm and point C is the center of gravity of upper arm BE. The vector G_1 is the weight of the moving platform $P_1P_2P_3P_4$ and point B is its center of gravity. The side length of platform is 2*lc*. The force $\vec{f}_1$ is exerted by the supporting bar on the platform. The length of the supporting bar is *lh* and the length of upper arm is *lu*. Points B_1 and B_2 overlap, so do points B_3 and B_4. The distance of B_1B_3 is 2*lb*. The platform is driven by four cables going through holes B_1 and B_3 and connecting to motors in the fixed base. To maintain static equilibrium of forces exerted on upper arm, the equation is

$$\sum_{i=1}^{4}(L_i/l_i \cdot t_i) + \vec{f}_1 + \vec{G}_1 + \vec{G}_2 - \vec{f}_4 + \sum_{j=5}^{6}(\vec{T}_{j1} + \vec{T}_{j2}) = 0_{3\times1} \quad (9)$$

To maintain static equilibrium of torques about point B, the equation is

$$\sum_{i=1}^{4}(\overrightarrow{BP_i} \times (L_i/l_i \cdot t_i)) + \overrightarrow{BC} \times \vec{G}_2 + \overrightarrow{BE} \times \left(-\vec{f}_4\right) + {\tau_1}^T + \overrightarrow{BQ}_5 \times \left(\vec{T}_{51} + \vec{T}_{52}\right) + \overrightarrow{BQ}_6 \times \left(\vec{T}_{61} + \vec{T}_{62}\right) = 0_{3\times1} \quad (10)$$

There are seven unknowns and six equations here. The seven unknowns are t1, t2, t3, t4 and three components of $\vec{f}_1$. This is also an underconstrained problem and the optimal solutions can be obtained by linear programming. The complete optimal solutions of cable tensions for the whole arm are available after statics analysis of the hand, the forearm and the upper arm. Next, a numerical example will be used here to test which design consumes the least cable tensions for the same pseudostatic motion (slow enough that acceleration of the motion is negligible) of the robotic arm.

Example 1: The robotic arm will perform a pseudostatic motion with rotations about 7 joints. In each joint, the angle changes from one limit to the other in the following range. $\theta_1 = [0^\circ, 10^\circ]$, $\theta_2 = [0^\circ, 20^\circ]$, $\theta_3 = [0^\circ, 20^\circ]$, $\theta_4 = [10^\circ, 25^\circ]$, $\theta_5 = [0^\circ, 10^\circ]$, $\theta_6 = [0^\circ, 20^\circ]$, $\theta_7 = [0^\circ, 25^\circ]$. The cycloidal function (Wiliams, 2009) is used to form an array of angles changing smoothly from one limit to the other.

$$\theta_i(t) = \theta_{i0} + (\theta_{iF} - \theta_{i0})\left(\frac{t}{t_F} - \frac{1}{2\pi}sin\frac{2\pi t}{t_F}\right) \quad (11)$$

where i is from 1 to 7; θ_{i0} and θ_{iF} is the first and second component of the motion range above, respectively; t is the time variable and t_F is the final time; t changes from 0 to 10 seconds, so this motion is slow and the acceleration of the motion is negligible. The common parameters of seven designs are listed as follows:

Density of material of mechanism: $\rho_{aluminum} = 2700\ kg/m^3$, lower bound cable tension: 5 N. In upper arm: *lh*=0.075 m, *lc*=0.05 m, *lu*=0.315m, radius of upper arm bar *r*=0.01 m, thickness of platform d_1=0.01 m. In forearm: EF=0.005 m, RE=0.04 m , $P_5F=P_6F$=0.03 m, *lf*=0.287 m, radius of forearm bar *r*=0.01 m. In hand: *lg*=0.04m, *lq*=0.025m, *lha*=0.105m, radius of hand bar *r*=0.01m, thickness of the platform d_2=0.005m.

The specific parameters for seven design are listed as follows: For Design 1A, *lb*=0.015m<*lc*, Q_5R=0.015m<P_5F, *lp*=0.01m<*lq*. For Design 1B, *lb*=0.05m=*lc*, Q_5R=0.03m=P_5F, *lp*=0.025m=*lq*. For Design 1C, *lb*=0.06m>*lc*, Q_5R=0.04m>P_5F, *lp*=0.03m>*lq*. For Design 2A, *lb*=0.015m<*lc*, Q_5R=0.015m<P_5F, *lp*=0.01m<*lq*. For Design 2B, *lb*=0.05m=*lc*, Q_5R=0.03m=P_5F, *lp*=0.025m=*lq*. For Design 2C, *lb*=0.06m>*lc*, Q_5R=0.04m>P_5F, *lp*=0.03m>*lq*.

Cable tensions for the whole cable-driven robotic arm can be obtained by simulations in Matlab. Comparing the cable tensions of Designs 1A, 1B and 1C, it is concluded that with length increase of *lb*, Q_5R and *lp*, the cable tensions needed for upper arm decrease greatly and tensions for other cables stay about the same, so Design 1C is the best design out of those three designs for using the least cable tensions to perform the same motion. Comparing the cable tensions of Designs 2A, 2B and 2C, it is similar that with length increase of *lb*, Q_5R and *lp*, the cable tensions needed for the upper arm decrease greatly and tensions for other cables stay about the same, so Design 2C is the best design out of those three designs for using the least cable tensions to perform the same motion. Design 1C uses even smaller cable tensions than Design 2C to perform the

same motion, so the best design for using the least cable tensions is Design 1C.

Actually, the trend of decrease of cable tensions with length increase of *lb*, Q_5R and *lp* is not a coincidence. Because of the special characteristics of this 3 DOF spherical joint, it is much harder to create torque in the z axis than torques in the x or y axes (see Fig. 6). Therefore, the design can produce the same torque in the z axis with less cable tensions is better. One cable tension in three different designs is analyzed in Fig. 6. It is disassembled in the x, y and z axes. In Design 1A (*lb*<*lc*), the component forces that affect torque in the z axis are T_x and T_y. The directions of torques provided by T_x and T_y are opposite, so the two torques will partially cancel out. In Design 1B (*lb*=*lc*), there is no component force in the x direction so the torque in z axis is only provided by component force T_y. In Design 1C (*lb*>*lc*), the torques provided by component forces T_x and T_y are in the same direction so the total torque is the sum of two torques. In order to provide the same torque about the z axis, the cable tension in Design 1C is the smallest. And producing torque in z axis is the hardest part of the motion, so that is why Design 1C uses the smallest cable tensions to perform the same motion.

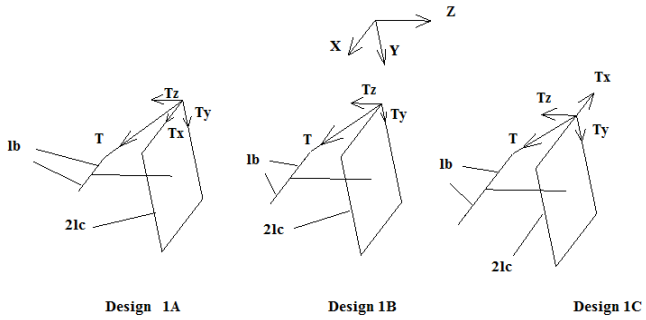

Figure 6. ANALYSIS OF TORQUES ABOUT THE Z AXIS

MOTION RANGE

It is known that Design 1C is the best design for the using the least cable tensions from the previous section. However, it is uncertain if its motion range is bigger than the other designs' or not. It is vital to always maintain a positive tension for every cable in a cable-driven mechanism, which can be used to find the practical motion range of this mechanism (Chen et al., 2006; Pham et al., 2004). The motion ranges of shoulder joint are calculated using the approach by MATLAB and shown in Fig. 7, 8 and 9.

The approximate volumes of motion ranges of shoulder joints of Designs 1A, 1B and 1C are 15, 8 and 7, respectively. It is also shown in the figures that the motion ranges of shoulder joint of Design 1A and 1C are the biggest and smallest out of three designs. Because the structures of shoulder joint and wrist joint are similar, the motion range of wrist joint of Design 1A is also bigger than that of Design 1C. Therefore Design lA has the biggest motion range out of three designs and Design 1C has the smallest one.

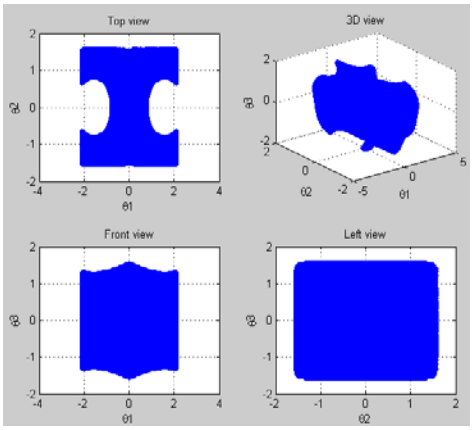

Figure 7. DES 1A SHOULDER JOINT MOTION RANGE

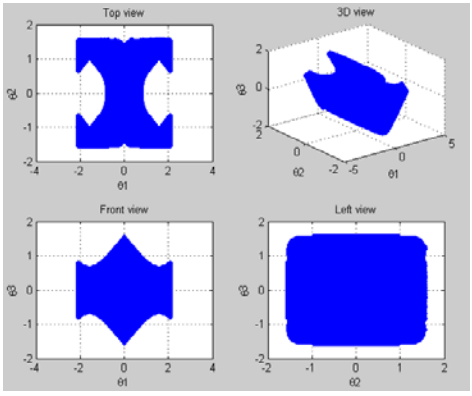

Figure 8. DES 1B SHOULDER JOINT MOTION RANGE

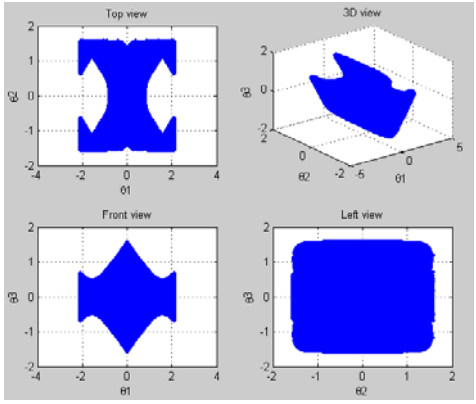

Figure 9. DES 1C SHOULDER JOINT MOTION RANGE

CABLE KINEMATICS ANALYSIS

Cable Kinematics represents the relationship between cable lengths and the end-effector pose of 7-DOF cable-driven robotic arm. It includes forward pose cable kinematics and inverse pose cable kinematics.

Forward Pose Cable Kinematics

Forward pose cable kinematics is used to get the end-effector pose of robotic arm given the lengths of the driving cables from moving platforms to corresponding motors in a fixed base. The 7-DOF cable-driven arm is shown in Fig. 10 and it is controlled by 10 cables connected with 10 motors (not

shown in the figure) in the base. The shoulder and wrist joints are the spherical joints (Design 1B). The elbow joint is a revolute joint driven by two cables.

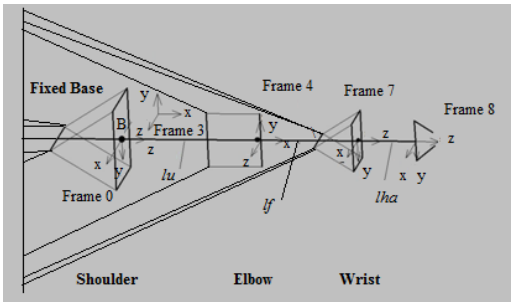

Figure 10. 7-DOF CABLE-DRIVEN ARM

A method (Yang, et al., 2005) is used here to implement forward pose cable kinematics of this model. According to the Section of Forward Pose Kinematics, the end-effector pose can be expressed by

$$ {}^0_8T = {}^0_3T \cdot {}^3_4T \cdot {}^4_7T \cdot {}^7_8T \qquad (12) $$

where ${}^7_8T = \begin{bmatrix} I_{3\times3} & {}^7_8P \\ 0 & 1 \end{bmatrix}$ and ${}^7_8P = [0 \quad 0 \quad lha]^T$; lha is the length of hand; ${}^0_3T$, ${}^3_4T$ and ${}^4_7T$ represent the pose of Frame 3 with respect to Frame 0, Frame 4 with respect to Frame 3, and Frame 7 with respect to Frame 4, respectively; ${}^0_3T = \begin{bmatrix} {}^0_3R & 0_{3\times1} \\ 1 & 0 \end{bmatrix}$, where ${}^0_3R$ is the rotational matrix of Frame 3 with respect to Frame 0; ${}^3_4T = \begin{bmatrix} {}^3_4R & {}^3_4P \\ 0 & 1 \end{bmatrix}$, where ${}^3_4R$ and ${}^3_4P$ are the rotational matrix and pose of Frame 4 with respect to Frame 3; ${}^3_4P = [lu \quad 0 \quad 0]^T$ and lu is the length of the upper arm; ${}^4_7T = \begin{bmatrix} {}^4_7R & {}^4_7P \\ 0 & 1 \end{bmatrix}$, where ${}^4_7R$ and ${}^4_7P$ are the rotational matrix and pose of Frame 7 with respect to Frame 4; ${}^4_7P = [lf \quad 0 \quad 0]$ and lf is the length of forearm. In Eqn. (12) only ${}^0_3R$, ${}^3_4R$ and ${}^4_7R$ are unknown. They are relative to rotational angles of seven frames which are also unknown, so obtaining ${}^0_3R$, ${}^3_4R$ and ${}^4_7R$ directly by those angles doesn't work. Finding the direct relationships between the cable lengths and rotational matrices is an appropriate approach.

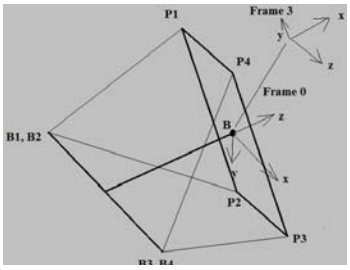

Figure 11. SHOULDER MODULE

There are three steps in forward pose cable kinematics of the whole arm. First, the relation between cable lengths and the end-effector pose in the shoulder joint is analyzed here. As shown in Fig. 11, the lengths of four cables--$\overline{B_1P_1}, \overline{B_2P_2}, \overline{B_3P_3}$ and $\overline{B_4P_4}$ are known because the bar B_1B_3 is attached to the base. The origins of Frames 0 and 3 are the same point B. Suppose that the coordinates of P_i and B_i (i=1, 2, 3, 4) with respect to Frame 0 are given by ${}^0P_{pi} = (x_{pi}, y_{pi}, z_{pi})$ and ${}^0P_{bi} = (x_{bi}, y_{bi}, z_{bi})$, respectively. Then the following equations are obtained by analysis:

$$ {x_{p3}}^2 + {y_{p3}}^2 + {z_{p3}}^2 = (\overline{BP_3})^2 $$
$$ (x_{p3} - x_{b3})^2 + (y_{p3} - y_{b3})^2 + (z_{p3} - z_{b3})^2 = (\overline{B_3P_3})^2 $$
$$ (x_{p1} - x_{b1})^2 + (y_{p1} - y_{b1})^2 + (z_{p1} - z_{b1})^2 = (\overline{B_1P_1})^2 $$

Because P_3 and P_1 are symmetric about point B and the coordinates of B with respect to Frame 0 is ${}^0P_b = (0, 0, 0)$, the coordinates of P_1 are also expressed as $(-x_{p3}, -y_{p3}, -z_{p3})$. Plug them into the equations above to replace the coordinates of P_1. Then for the three equations above, the only unknowns are the coordinates of P_3 (x_{p3}, y_{p3}, z_{p3}). At most two sets of solutions can be found by solving those three equations. Similarly, two sets of solutions for the coordinates of P_2 (x_{p2}, y_{p2}, z_{p2}) can be obtained. The distance between P_2 and P_3 $(\overline{P_2P_3})$ is known, which can been used to check the solutions for those two points. Normally, only one set of solutions for P_2 and one set of solutions for P_3 are valid. Suppose that the known coordinates of P_i with respect to Frame 3 are ${}^3P_{pi} = ({}^3x_{pi}, {}^3y_{pi}, {}^3z_{pi})$. The connections between ${}^0P_{pi}$ and ${}^3P_{pi}$ are:

$$ {}^0P_{p3} = {}^0_3R\,{}^3P_{p3} $$
$$ {}^0P_{p2} = {}^0_3R\,{}^3P_{p2} $$
$$ {}^0P_{p3} \times {}^0P_{p2} = {}^0_3R({}^3P_{p3} \times {}^3P_{p2}) $$

So ${}^0_3R$ can be obtained by

$$ {}^0_3R = \left[{}^0P_{p3} \quad {}^0P_{p2} \quad {}^0P_{p3} \times {}^0P_{p2}\right]\left[{}^3P_{p3} \quad {}^3P_{p2} \quad {}^3P_{p3} \times {}^3P_{p2}\right]^{-1} $$

With known ${}^0_3R$, ${}^0_3T$ in Eqn. (12) is known.

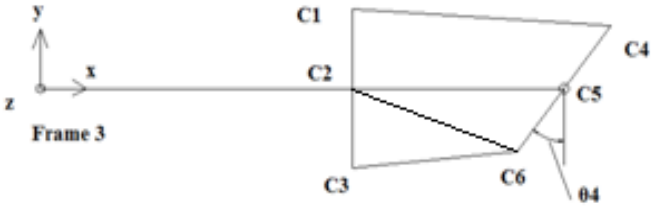

Figure 12. ELBOW MODULE

Second, the relationship between cable lengths and end-effector pose in the elbow joint is analyzed here. With known ${}^0_3T$ and coordinates of C_3 in Frame 3 in Fig. 12, the coordinates of C_3 in Frame 0 (base frame) is known so the cable length between C_3 and the corresponding motor in the base is known. Therefore, cable length $\overline{C_3C_6}$ can be obtained by subtracting the cable length between C_3 and the motor from the known total cable length. Cable length $\overline{C_1C_4}$ can be obtained by a similar method. Because the revolute joint on the elbow can only rotate

about z axis in Fig. 12, so the coordinates of all points in z axis are the same. In order to simplify the problem, the z coordinates of all points will not be shown in the analysis. Suppose that the coordinates of C_6 are $P_{c6} = (x_{c6}, y_{c6})$ with respect to Frame 3. The known coordinates of C_i (i=1, 2, 3, 5) with respect to Frame 3 are $P_{ci} = (x_{ci}, y_{ci})$. For this mechanism, the equations are obtained by analysis:

$$(x_{c6} - x_{c5})^2 + (y_{c6} - y_{c5})^2 = (\overline{C_5C_6})^2$$
$$(x_{c6} - x_{c3})^2 + (y_{c6} - y_{c3})^2 = (\overline{C_3C_6})^2$$

At most two sets of solutions of coordinates for C_6 can be obtained by solving two equations above. Only one set of solutions can be proved to be the real solution by checking the length of the other cable, so $\overline{C_2C_6}$ is obtained with known coordinates of C_6. In $\Delta C_2C_5C_6$, θ_4 can be calculated by the cosine law:

$$\theta_4 = \frac{\pi}{2} - \cos^{-1}\left(\frac{(\overline{C_2C_5})^2 + (\overline{C_5C_6})^2 - (\overline{C_2C_6})^2}{2\overline{C_2C_5} \cdot \overline{C_5C_6}}\right)$$

Since θ_4 is known, the transformation matrix ${}^3_4T$ can be obtained.

Third, with known ${}^3_4T$, ${}^0_3T$ and the coordinates of guiding holes of bar for wrist in Frame 4 in Fig. 10, the lengths of the cables from the moving platform of wrist to the guiding holes of its bar can be obtained by a similar method mentioned in elbow. Because the shoulder and wrist joints are similar spherical joints, the solutions for them are similar. The transformation matrix for the wrist joint ${}^4_7T$ can be obtained by a similar method. With known ${}^0_3\mathrm{T}$, ${}^3_4\mathrm{T}$, ${}^4_7\mathrm{T}$ and ${}^7_8\mathrm{T}$, ${}^0_8\mathrm{T}$ can be obtained by Eqn. (12) and the pose of end-effector is obtained. So forward pose cable kinematics of the whole arm is finished.

Inverse Pose Cable Kinematics (IPCK)

Inverse pose cable kinematics is calculation of the required cable lengths given the end-effector pose. Since this process is difficult, it is divided into two steps. First, use inverse pose kinematics to find optimal rotational angles in each frame with the known pose of the end-effector. Inverse pose kinematics for 7-DOF redundant arm model has been published by Tarokh et al. (2010), so the details of that method will not be discussed here. Second, calculate the cable lengths with known optimal rotational angles in each frame (Chen et al., 2006). With those two steps, IPCK can be accomplished.

DYNAMICS ANALYSIS

Dynamics analysis considers not only forces and torques applied on the system like statics analysis, but also the effects of motion to the system including translational and rotational accelerations of the system.

Dynamics Analysis of the Cable-Driven Robotic Arm

The dynamics analysis of the whole robotic arm is also done part by part. First, the hand is analyzed; its free body diagram is shown in Fig. 13. There are only two new variables in the figure: a_1 and α_1, where a_1 is the acceleration of the hand and platform and α_1 is the angular acceleration of the hand and platform about a ball joint I. Both of them are calculated with respect to the fixed Frame 0. The rest of the variables are the same with those in statics analysis of the hand. The equation of forces exerted on the hand can be expressed by

$$\sum_{i=7}^{10}(\mathrm{L}_i/\,\mathrm{l}_i \cdot \mathrm{t}_i) + \overrightarrow{\mathrm{f}_6} + \overrightarrow{\mathrm{G}_5} + \overrightarrow{\mathrm{G}_4} = (\mathrm{m}_5 + \mathrm{m}_4)\overrightarrow{\mathrm{a}_1} \quad (13)$$

where m_4 is the mass of platform and m_5 is the mass of hand. Use forward pose kinematics to calculate the pose of the center of gravity (CG) of hand and platform—s_1 with respect to Frame 0. The acceleration of the hand $\overrightarrow{a_1}$ is obtained by taking the second time derivative of s_1. The equation of torques about point I can be expressed by

$$\sum_{i=7}^{10}(\overrightarrow{\mathrm{IQ}_i} \times (\mathrm{L}_i/\,\mathrm{l}_i \cdot \mathrm{t}_i)) + \overrightarrow{\mathrm{IJ}} \times \overrightarrow{\mathrm{G}_5} = \left(\mathrm{I}_5 + \mathrm{I}_{\mathrm{p1}}\right)\alpha_1 \quad (14)$$

where I_5 and I_{p1} are the inertia tensors of the hand and platform $Q_7Q_8Q_9Q_{10}$ expressed in Frame 7, respectively. Newton-Euler dynamics equations (Craig, 2005) are used where the iterations are done from *i*=0 to 6; Because Frame 0 is a fixed frame, its angular velocity ${}^0\omega_0$ and angular acceleration ${}^0\alpha_0$ with respect to its own frame are both equal to $[0 \quad 0 \quad 0]^{\mathrm{T}}$; ${}^{i+1}_iR$ is the rotational matrix of Frame *i* based on Frame *i*+1 and it is the inverse (transpose) matrix of ${}^i_{i+1}R$; ${}^i\omega_i$ and ${}^i\alpha_i$ are the angular velocity and angular acceleration of Frame *i* based on its own frame, respectively. After iterations ${}^7\alpha_7, {}^6\alpha_6, {}^5\alpha_5, {}^4\alpha_4, {}^3\alpha_3, {}^2\alpha_2$ and ${}^1\alpha_1$ are available. The angular acceleration of the hand α_1 can be obtained by:

$$\alpha_1 = {}^0\alpha_7 = {}^0_7R\,{}^7\alpha_7 \quad (15)$$

Then linear programming is used to obtain the optimal solutions of four cable tensions and the solutions of $\overrightarrow{\mathrm{f}_6}$.

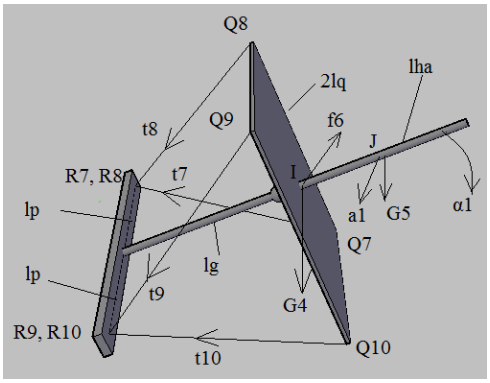

Figure 13. HAND FBD

Second, the forearm is analyzed; its free body diagram is shown in Fig. 14. There are two new variables in the figure: a_2 and α_2, where a_2 represents the acceleration of the forearm and α_2 represents the angular acceleration of the forearm. Both are calculated with respect to Frame 0. The rest of variables in the figure are the same with those in statics analysis of the forearm.

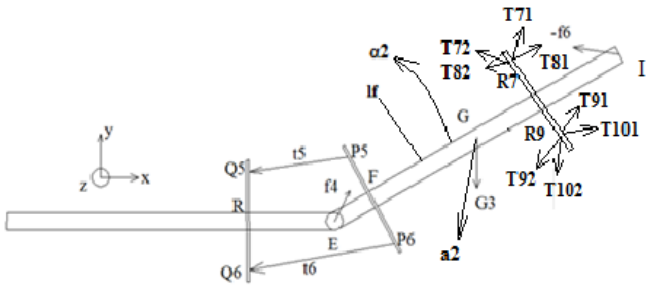

Figure 14. FOREARM FBD

The equation of forces exerted on the forearm is:

$$\sum_{i=5}^{6}(L_i/\,l_i \cdot t_i) + \overrightarrow{G_3} + \overrightarrow{f_4} - \overrightarrow{f_6} + \sum_{j=7}^{10}(\overrightarrow{T}_{j1} + \overrightarrow{T}_{j2}) = m_3\overrightarrow{a_2} \quad (16)$$

where m_3 is the mass of the forearm. The mass of beam P_5P_6 is negligible. The equation of torques about point E is

$$\left\{\sum_{i=5}^{6}(\overrightarrow{EP_i} \times (L_i/\,l_i \cdot t_i)) + \overrightarrow{EG} \times \overrightarrow{G_3} + \overrightarrow{EI} \times (-\vec{f}_6) + \overrightarrow{ER_7} \times \sum_{j=7}^{8}(\overrightarrow{T}_{j1} + \overrightarrow{T}_{j2}) + \overrightarrow{ER_9} \times \sum_{k=9}^{10}(\overrightarrow{T}_{k1} + \overrightarrow{T}_{k2})\right\}^{T} \cdot \begin{bmatrix}0\\0\\1\end{bmatrix} = (I_3\alpha_2)^{T} \cdot \begin{bmatrix}0\\0\\1\end{bmatrix} \quad (17)$$

where I_3 is the inertia tensor of the forearm with respect its own frame. Because the revolute joint E can only provide torques in z axis in Fig. 14, Eqn. (17) only contains torques in z axis. The angular acceleration of forearm about point E α_2 can be obtained by

$$\alpha_2 = {}^0\alpha_4 = {}^0_4R^4\alpha_4 \quad (18)$$

Using Eqn. (16), (17) and (18), the optimal solutions of cable tensions and solutions of $\overrightarrow{f_4}$ can be obtained by linear programming. Then the torques in the x and y axes transferred by the revolute joint to the upper arm can be calculated by

$$\tau_1 = \left\{\sum_{i=5}^{6}(\overrightarrow{EP_i} \times (L_i/\,l_i \cdot t_i)) + \overrightarrow{EG} \times \overrightarrow{G_3} + \overrightarrow{EI} \times (-\vec{f}_6) + \overrightarrow{ER_7} \times \sum_{j=7}^{8}(\overrightarrow{T}_{j1} + \overrightarrow{T}_{j2}) + \overrightarrow{ER_9} \times \sum_{k=9}^{10}(\overrightarrow{T}_{k1} + \overrightarrow{T}_{k2}) - I_3\alpha_2\right\}^{T} \cdot \begin{bmatrix}1&0&0\\0&1&0\\0&0&0\end{bmatrix} \quad (19)$$

where τ_1 is a 3×1 matrix. The first two components of τ_1 are the torques in the x and y axes expressed in Frame 3 of the arm model. The third component is set to be zero because torques in the z axis can be balanced by the revolute joint.

Third, the upper arm is analyzed; its free body diagram is shown in Fig. 15. There are also two new variables in the figure: a_3 and α_3, where a_3 is the acceleration of the upper arm and platform, and α_3 is the angular acceleration of the upper arm and platform. Both are calculated with respect to Frame 0. The rest of variables are the same with those in the statics analysis of the upper arm. The equation of forces exerted on the upper arm can be expressed by

$$\sum_{i=1}^{4}(L_i/\,l_i \cdot t_i) + \overrightarrow{f_1} + \overrightarrow{G_1} + \overrightarrow{G_2} - \overrightarrow{f_4} + \sum_{j=5}^{6}(\overrightarrow{T}_{j1} + \overrightarrow{T}_{j2}) = (m_2 + m_1)\overrightarrow{a_3} \quad (20)$$

where m_2 is the mass of the upper arm and m_1 is the mass of the platform $P_1P_2P_3P_4$.

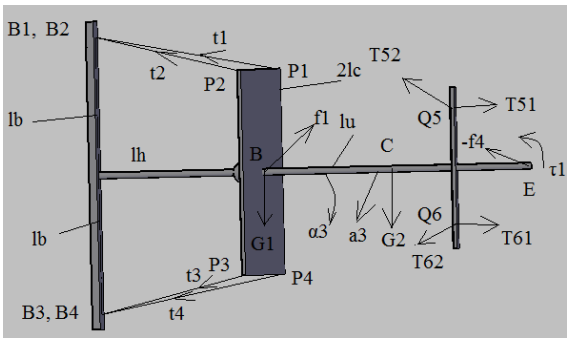

Figure 15. UPPER ARM FBD

The equation of torques about the ball joint B can be expressed by

$$\sum_{i=1}^{4}(\overrightarrow{BP_i} \times (L_i/\,l_i \cdot t_i)) + \overrightarrow{BC} \times \overrightarrow{G_2} + \overrightarrow{BE} \times (-\overrightarrow{f_4}) + {\tau_1}^T + \overrightarrow{BQ_5} \times (\overrightarrow{T}_{51} + \overrightarrow{T}_{52}) + \overrightarrow{BQ_6} \times (\overrightarrow{T}_{61} + \overrightarrow{T}_{62}) = (I_2 + I_{p2})\alpha_3 \quad (21)$$

where I_2 and I_{p2} are the inertia tensors of the upper arm and the platform with respect to Frame 3, respectively. The angular acceleration of the upper arm and platform α_3 is obtained by

$$\alpha_3 = {}^0\alpha_3 = {}^0_3R^3\alpha_3 \quad (22)$$

With Eqn. (20), (21) and (22), the optimal solutions of cable tensions and solutions of $\overrightarrow{f_1}$ can be obtained by linear programming. Therefore, dynamics analysis of the whole arm is accomplished. Design 1B will be used for dynamics analysis to perform the same motion in the Example 1 of statics analysis.

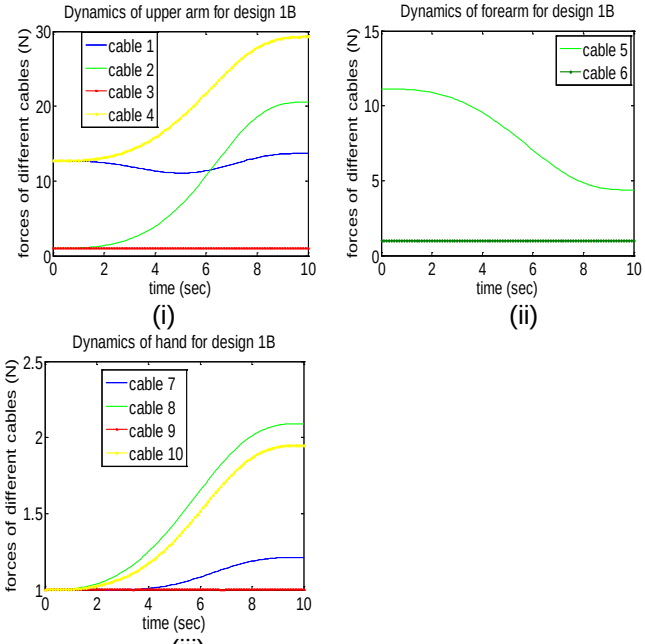

Figure 16. SLOW DYNAMICS CABLE TENSIONS

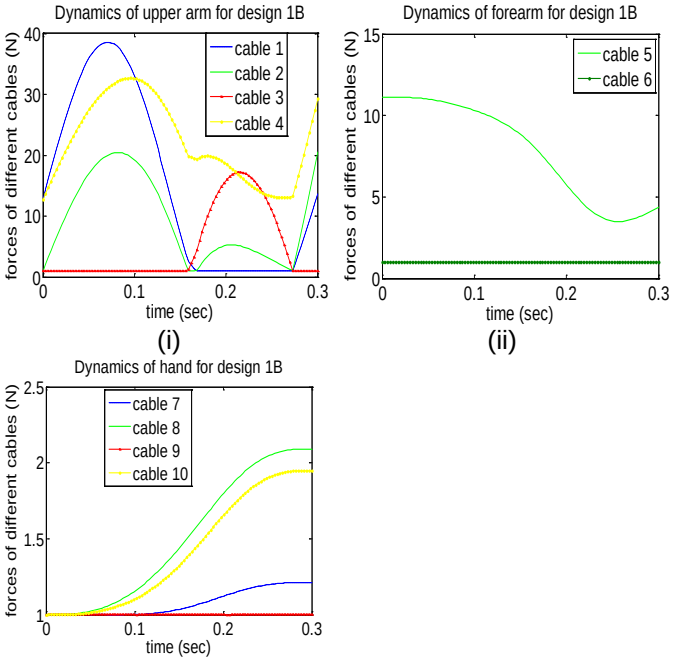

Figure 17. FAST DYNAMICS CABLE TENSIONS

When the total time t_F=10 sec (slow motion), the optimal cable tensions of dynamics analysis are shown in Fig. 16. When t_F =0.3 sec (fast motion), the optimal cable tensions of dynamics analysis are shown in Fig. 17. Comparing Fig. 16 with Fig. 17, it is proved that cable tensions of fast motion are greater than those of slow motion.

Dynamics Analysis of Motor-Driven Robotic Arm

Typically, motors of traditional motor-driven robotic arm are directly installed at each joint. The motors are moving with the robot, so it has the following disadvantages: heavy, slow response and low load capacity. The arm model in real world is shown in Fig. 18. In the figure, *d* is the distance between two frames in a spherical joint. Suitable motors are selected based on their abilities of generating motions needed in different joints. The weights of those motors are considered in dynamics because they are heavy and they greatly affect the motion of the arm. For this traditional robotic arm with 7 DOF, seven motors are needed because one motor generates 1 DOF motion.

Next, iterative Newton-Euler dynamics algorithm (Craig, 2005) is employed for dynamics analysis of the arm model shown in Fig.18. It includes two steps: outward iterations and inward iterations. After those iterations, τ_i that is the torque needed from the motor in frame *i* is obtained (*i*=1, 2, 3, 4, 5, 6, 7). The energy needed for each frame can be calculated by:

$$E_i = \int_{\theta_i=\theta_{i0}}^{\theta_{if}} \tau_i d\theta_i \qquad (23)$$

where τ_i is the torque needed in frame *i* (*i*=1, 2, 3, 4, 5, 6, 7); θ_i is the rotational angle in frame *i* and it is expressed in radians; θ_{i0} is the initial angle and θ_{if} is the final angle for frame *i*.

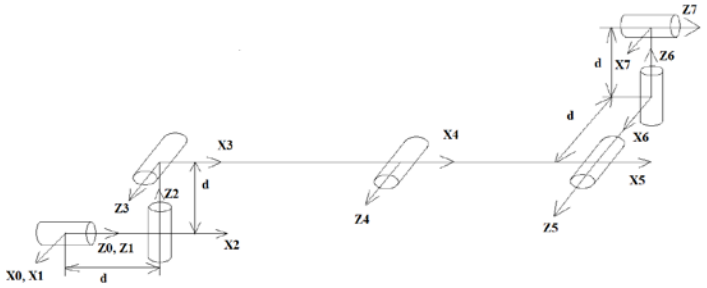

Figure 18. 7-DOF ARM MODEL IN REAL WORLD

.

In order to finish the same motion mentioned in statics analysis, total energy of seven motors is shown in following cases:

a) Slow motion: t_F=10 sec, d=0.05m. (Fig. 19)
b) Fast motion: t_F=0.3 sec, d=0.05m. (Fig. 20)

From Fig. 19 and 20, the total energy consumptions of all motors in fast motion and slow motion of the same path are about the same (3.7 J) because the changes of the total energy (potential energy and kinetic energy) of the motor-driven robotic arm in both motions are about the same.

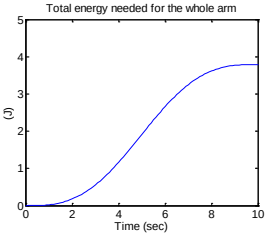

Figure 19. TRADITIONAL SLOW DYNAMICS ENERGY

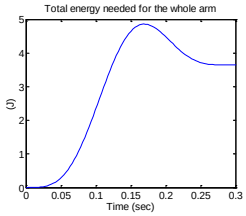

Figure 20. TRADITIONAL FAST DYNAMICS ENERGY

Comparison of Cable-Driven and Motor-Driven Robot

This section will compare the consumptions of energy and power of cable-driven robot and traditional motor-driven robot to perform the same motion in Example 1.

First, total energy consumptions of both robots are compared. Since the cable tensions of cable-driven robot are obtained in dynamics analysis, its total energy consumption for each cable is:

$$E_j = \int_{c_j} t_j ds_j \qquad (24)$$

where t_j is tension of cable *j* (*j*=1, 2, 3, 4, 5, 6, 7, 8, 9, 10); s_j is the pose of cable *j*; c_j is the path of the pose of cable *j*. The method of calculating cable lengths was proposed by Chen et al. (2006). For slow motion (t_F=10sec), the total energy needed for two different robots is shown in Fig. 21.

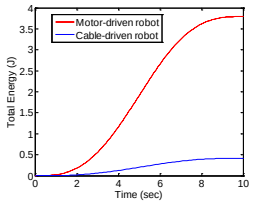

Figure 21. SLOW MOTION ENERGY COMPARISON

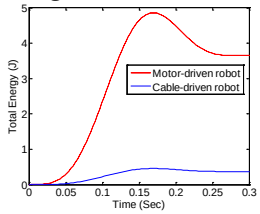

Figure 22. FAST MOTION ENERGY COMPARISON

From Fig. 21, it is shown that even in slow motion the total energy needed for the cable-driven robot is about 1/9 of that needed for the motor-driven robot. That means cable-driven robot is better than motor-driven robot in saving energy to perform the same slow motion. For fast motion (t_F=0.3sec), the total energy needed for two different robots is shown in Fig 22. From the figure, it is shown that in fast motion the total energy needed for the cable-driven robot is only about 1/10 of that needed for the motor-driven robot. That means in the same fast motion the cable-driven robot performs far better than the motor-driven robot in saving energy.

Second, power consumptions of both robots are compared. The instantaneous power can be obtained by:

$$P = \frac{dE}{dt} \approx \frac{\Delta E}{\Delta t} \qquad (25)$$

where E is the energy needed for the motion and t is time. For slow motion ($t_F = 10\text{sec}$ and $\Delta t = 0.1$ sec), the total instantaneous power needed for two different robots is shown in Fig. 23. For fast motion ($t_F = 0.3$sec and $\Delta t = 0.003$ sec), the total instantaneous power needed for two different robots is shown in Fig. 24.

In Fig. 23, the maximum total instantaneous power of cable-driven robot is about 1/10 of that of motor-driven robot in the same slow motion. In Fig. 24, the maximum total instantaneous power of cable-driven robot is less than 1/10 of that of motor-driven robot in the same fast motion. It proves that cable-driven robot is much better than motor-driven robot for saving power in both slow motion and fast motion.

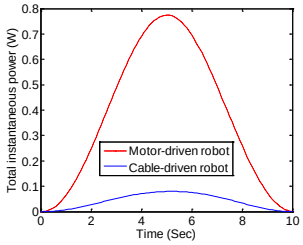

Figure 23. SLOW MOTION POWER COMPARISON

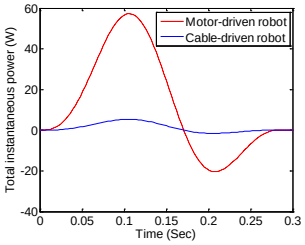

Figure 24. FAST MOTION POWER COMPARISON

CONCLUSIONS

This paper focuses on mechanism design, kinematics and dynamics analysis of a 7-DOF cable-driven humanoid robotic arm. The relations among rotational angle θ, pose of end-effector x, rotational velocity ω ($\omega = \dot{\theta}$), velocity of end-effector $\dot{x}$ and cable length L are discussed.

Forward pose kinematics, forward velocity kinematics and inverse velocity kinematics are discussed. The general redundant solution is introduced. Seven designs are presented based on a design proposed in the literature. In statics analysis Design 1C uses the smallest cable tensions out of those designs to perform the same motion and Design 1A has the biggest motion range out of Designs 1A, 1B and 1C. The relationships between cable lengths and end-effector pose are also analyzed. Dynamics analysis of the cable-driven robot and the traditional robot are implemented. It is concluded that the cable-driven robot needs much less energy and much smaller power than traditional motor-driven robot in the same motion.

ACKNOWLEDGMENTS

The authors thank Ohio University graduate student Elvedin Kljuno for his advice in cable-driven robot analysis.

REFERENCES

Borgstrom, P. H., Jordan, B. L., Sukhatme, G. S., Batalin, M. A., Kaiser, W. J. (2009). Rapid computation of optimally safe tension distributions for parallel cable-driven robots. IEEE Transactions on Robotics, Vol. 25, NO. 6.

Chen, W., Chen, Q., Zhang, J., Yu, S. (2006). Kinematics control for a 7-dof cable-driven anthropomorphic arm. Proceedings of the 2006 IEEE/RSJ International Conference on Intelligent and Systems, 1650-1655.

Craig, J.J. (2005). Introduction to robotics: mechanics and control (3rd ed.). Upper Saddle River, NJ: Addison-Wesley Publishing Company.

Liegeois, A. (1977). Automatic supervisory control of the configuration and behavior of multibody mechanisms. IEEE Trans. Syst., Man, 7,866-871.

Pham, C.B., Yeo, S.H., Yang, G. (2004). Workspace analysis and optimal design of cable-driven planar parallel manipulators. Proceedings of the 2004 IEEE Conference on Robotics, Automation and Mechatronics, 219-224.

Tarokh, M., Keerthi, K., Lee, M. (2010). Classification and characterization of inverse kinematics solutions for anthropomorphic manipulators. Robotics and Autonomous Systems 58, 115-120.

Venkatayogi, C. (2007). Simulation of a humanoid robot. MS Thesis, Mechanical Engineering, Ohio University, Advisor Robert L. Williams II.

Williams, R.L. II. (1992). Kinematic equations for control of the redundant eight-degree-of-freedom advanced research manipulator II. NASA Technical Memorandum 4377,1-25.

Williams, R.L. II. (1994). Local performance optimization for a class of redundant eight-degree-of-freedom manipulators. NASA Technical Paper 3417, 1-21.

Williams, R.L. II, Bosscher, P., Bryson, L.S., Castro-Lacouture, D. (2006). Cable-suspended robotic contour crafting system. Proceedings of IDETC/CIE 2006 ASME 2006 International Design Engineering Technical Conferences and Computers and Information in Engineering Conference September 10-13, 2006, Philadelphia, Pennsylvania, USA.

Williams, R.L. II. (2009). ME 467 / BME 567 Engineering Biomechanics of Human Motion Class Notes, Ohio University, Athens, OH, USA.

Yang, G., Lin, W., Kurbanhusen, M.S., Pham, C.B., Yeo, S.H. (2005). Kinematic design of a 7-dof cable-driven humanoid arm: a solution-in-nature approach. Proceedings of the 2005 IEEE/ASME International Conference on Advanced Intelligent Mechatronics, 444-449.